Modeling the High Temperature Flow Behavior and Dynamic Recrystallization Kinetics of a Medium Carbon Microalloyed Steel

Mahmoud Reza Ghandehari Ferdowsi, Davood Nakhaie, Pooya Hosseini Benhangi, and Gholam Reza Ebrahimi

In this study, the hot deformation behavior of a medium carbon microalloyed steel was investigated. The hot compression test was conducted in the temperature range of 1000-1200 °C under strain rates of 0.01, 0.1 and 1 s^{-1}. It has been observed that the flow stress increases with a decrease in temperature and/or an increase in strain rate. Furthermore, dynamic recrystallization (DRX) is found to be the main flow softening mechanism in almost all deformation conditions. Material parameters of the constitutive equations are found to be strain dependent. Their relationship with strain is identified by a fourth order polynomial fit. Then, a constitutive model is developed to predict the flow stress of the material incorporating the strain softening effect. The accuracy of the proposed model for the flow stress is evaluated by applying the absolute average error method. The result of 6.08% indicates a good agreement between predicted and experimental data. Moreover, the critical characteristics of DRX are extracted from the stress-strain curves at different deformation conditions. It is found that by increasing the strain rate at a constant temperature or decreasing deformation temperature under a constant strain rate, the recrystallization curve shifts to the higher strains. The kinetics of DRX increases with increasing deformation temperature or strain rate.

1. Introduction

The flow behavior of metals and alloys at elevated temperatures is of great importance for industrial hot deformation processing. Recently, finite element (numerical) simulation as an efficient approach for the evaluation of the hot plastic deformability of metallic materials and the optimization of deformation conditions has been extensively applied to the study of metal plastic-forming processes (Ref 1-3). The numerical simulation can be reliable only when a proper constitutive equation is inserted into the finite element code as input data. These equations correlate thermomechanical processing parameters such as flow stress, strain, strain rate and temperature with each other.

So far, various models have been proposed by different researchers to predict the flow behavior during hot deformation for a wide variety of metals and alloys. As is well known, the exponential type equation has been widely adopted for establishing constitutive models (Ref 4, 5). However, this equation is inappropriate at low stresses. In another approach, Sellars and McTegart (Ref 6) proposed a hyperbolic-sine Arrhenius equation to describe the high temperature flow behavior of materials over a wide range of stresses. This kind of equation was used by other researchers for predicting the flow stress of various metals and alloys (Ref 7, 8). It should be noted that in the majority of previous studies on the constitutive analysis of hot flow behavior of materials, only the effect of deformation temperature and strain rate was taken into account. However, the influence of strain has not been considered for the development of the constitutive model. In order to incorporate the effect of strain on the constitutive model, Rao et al. (Ref 9) introduced a strain-dependent parameter into the hyperbolic-sine Arrhenius equation. Recently, a revised hyperbolic sine constitutive equation has been proposed to predict the high temperature flow behavior by considering strain compensation (Ref 4, 10-13). This model has been employed by various researchers to formulate the constitutive behaviors of 42CrMo steel (Ref 4), $Cr_{20}Ni_{25}Mo_4Cu$ superaustenitic stainless steel (Ref 12), Ti-modified austenitic stainless steel (Ref 13), AZ81 magnesium alloy (Ref 11) and Ti-6Al-4V alloy (Ref 10).

It is well known that work hardening and dynamic softening occur frequently during the hot deformation of metals and alloys. The two main restoration mechanisms are dynamic recovery (DRV) which leads to annihilation and rearrangement of dislocations, and DRX which results in the formation of new strain-free grains. In low stacking fault energy metals [such as the austenite phase in steels (Ref 14)], the ability of dislocations to climb and/or cross slip is hindered. Thus, in these materials DRV is suppressed and DRX acts as the major restoration mechanism during hot deformation processes (Ref 15-17). On the other hand, DRX dominates the microstructure and thus dictates the mechanical properties during hot deformation

Mahmoud Reza Ghandehari Ferdowsi, Davood Nakhaie, and **Pooya Hosseini Benhangi**, Department of Materials and Metallurgical Engineering, Faculty of Engineering, Ferdowsi University of Mashhad, P.O. box 91775-1111, Mashhad, Iran; and **Gholam Reza Ebrahimi**, Department of Materials and Polymers Engineering, Faculty of Engineering, Hakim Sabzevari University, Sabzevar, Iran. Contact e-mail: reza.ghandehari.f@gmail.com.

processing. Therefore, it can be concluded that the DRX behavior of austenite is of great importance during thermomechanical processing of steels.

During hot deformation, DRX can be initiated at a critical level of stress accumulation (Ref 18). The softening due to DRX causes the strain hardening rate to decrease, generating a peak on the flow curve at which the strain hardening rate equals zero. Although the existence of a peak on the flow curve indicates the formation of new grains, DRX actually starts at a critical strain (ε_c) which is lower than the strain at peak stress (ε_p) (Ref 19, 20). This critical strain is a function of initial microstructure and deformation conditions (Ref 21). So far, many studies have been conducted to study the typical behavior of DRX (Ref 22-24) as well as the kinetics of DRX (Ref 20, 25-27).

In this study, a strain dependent constitutive relationship for a medium carbon microalloyed steel was developed by utilizing the experimental data obtained from isothermal hot compression tests. The accuracy of the developed constitutive model was verified over the entire experimental range. Furthermore, the critical characteristics of DRX, including critical and peak strain, were determined using the work hardening rate versus true stress under different hot deformation conditions. Finally, the kinetics of DRX was analyzed by constructing the curve of recrystallized volume fraction based on the flow curves.

2. Experimental Procedure

The chemical composition (wt.%) of the investigated steel and its microstructure are shown in Table 1 and Fig. 1, respectively. The microstructure consists of relatively fine ferrite grains and pearlite colonies.

Cylindrical hot compression specimens, 12 mm in height and 8 mm in diameter [in accordance with ASTM E209 (Ref 28) were machined from a stock of material. In order to dissolve carbonitride precipitates (Ref 29), the specimens were heated up to 1200 °C in a separate resistance furnace and held isothermally for 5 min. After soaking, the specimens were moved immediately to the testing machine, a Zwick/Roell-250 machine equipped with a resistance furnace. To ensure that the temperature became homogeneous throughout the specimens during the hot compression test, they were held there for 5 min prior to straining. The hot compression tests were performed in the temperature range of 1000-1200 °C, at an interval of 50 °C, under constant strain rates of 0.01, 0.1 and 1 s^{-1}, up to the true strain of 0.9. Upon completion of the hot compression test, the specimens were immediately quenched in tap water. The thermomechanical processing schedule is schematically shown in Fig. 2.

3. Results and Discussion

3.1 Analysis of Hot Flow Curves

The effect of strain rate and deformation temperature on the true stress-true strain curves of the investigated steel is shown in Fig. 3. It can be seen that these processing parameters (temperature and strain rate) have a remarkable impact on the flow curves. The flow stress level decreases with increasing compression temperature and/or decreasing strain rate. It is assumed that the formation of dislocations and their accumulation behind the barriers reduces the dislocation movements which, in turn, causes the flow stress to increase.

Moreover, it can be clearly observed that almost all flow curves exhibit a peak followed by a gradual decline to a steady state stress which is indicative of the occurrence of DRX, except for the specimens deformed at 1000 and 1050 °C under the strain rate of 1 s^{-1}. At the initial stage of straining, work hardening predominates and the flow stress exhibits a rapid increase up to a critical value with increasing strain. At the critical strain, where the driving force for DRX is attained, new grains start to nucleate which, in turn, results in a gradual decrease in the hardening rate.
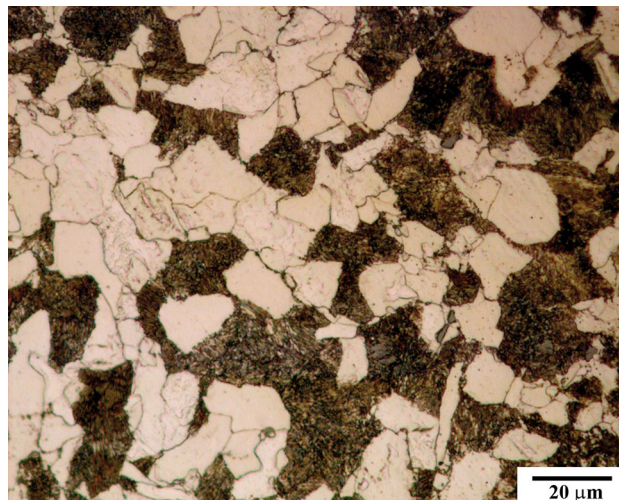

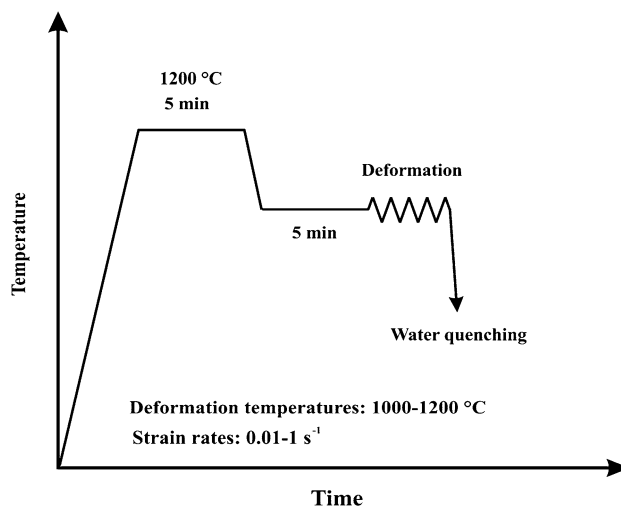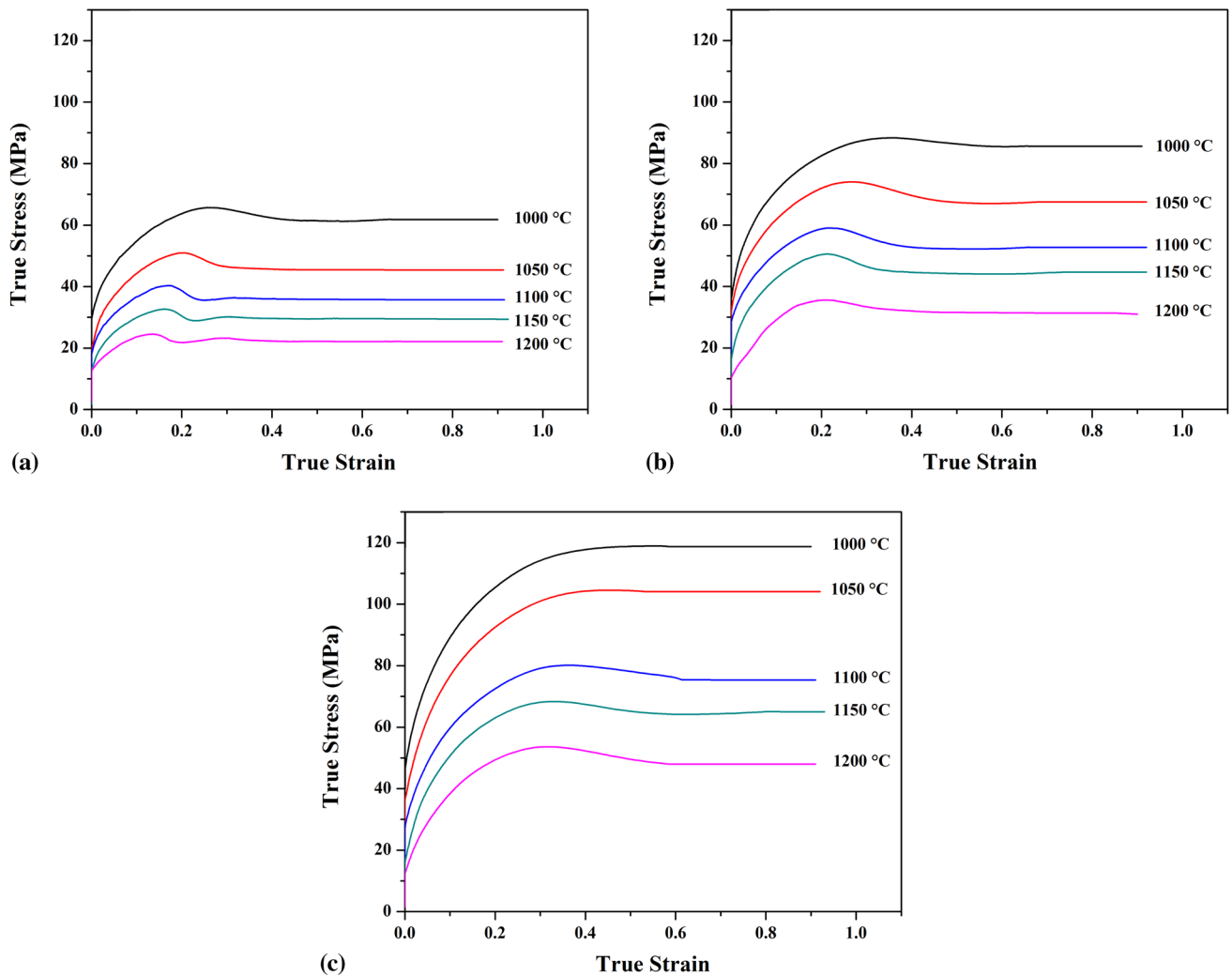**Fig. 1** The optical microstructure of the as-received material

Fig. 2 A schematic diagram of the thermomechanical processing schedule

Table 1 Chemical composition (in wt.%) of the investigated steel

C	Mn	Si	S	P	Nb	V	Ti	Cr	Al	N	Fe
0.241	1.538	0.287	0.028	0.011	0.049	0.120	0.002	0.197	0.026	0.013	Bal.

Fig. 3 The true stress-true strain curves of microalloyed steel compressed at different temperatures under strain rates of (a) 0.01, (b) 0.1 and (c) 1 s^{-1}

When the hardening rate becomes equal to the softening rate, the peak flow stress is reached. The flow softening beyond the peak stress, which is attributed to DRX (Ref 30), exceeds the hardening, thus, the stress drops gradually. Finally, the flow stress becomes steady when a new balance between softening rate and hardening rate is obtained.

For the case of the specimens deformed at 1000 and 1050 °C under the strain rate of 1 s^{-1}, DRX conditions were apparently not achieved. Thus, one may conclude that the non-recrystallization temperature (T_{NR}) for this microalloyed steel is below 1000 °C when compressed under a strain rate of 1 s^{-1}. It has been reported (Ref 14, 31) that the dynamic strain induced precipitation occurs during deformation at temperatures lower than T_{NR} in microalloyed steels. This precipitation is in turn responsible for the formation of pancaked austenite grains during deformation by hindering the occurrence of DRX (Ref 31). Furthermore, it can be concluded that the softening behavior during deformation at deformation temperatures close to T_{NR} results from the counteracting effects of restoration mechanisms and work hardening of austenite (Ref 32).

In addition, at the deformation temperatures of 1100, 1150 and 1200 °C under the strain rate of 0.01 s^{-1} (Fig. 3a), multiple peak flow appears in contrast with single peak flow

in other deformation conditions. It should be mentioned that such cyclic flow behavior is associated with grain coarsening during DRX (Ref 33). However, below the temperature of 1100 °C, only single peak behavior is recorded which is indicative of grain refining during DRX. It is well reported that increases in strain rate or reductions in the deformation temperature lead to the single peak behavior (Ref 33).

According to Fig. 3, at a constant strain rate, the peak stress and peak strain decrease with an increase in temperature. On the other hand, at a constant deformation temperature, the peak stress and peak strain decrease with a reduction of strain rate. It is well-known that higher temperatures and lower strain rates can promote the softening process by increasing the mobility of grain boundaries and providing longer time for dislocation annihilation and occurrence of DRX (Ref 12).

3.2 Evaluation of the Constitutive Model

The stress-strain data obtained from compression tests under different strain rates and temperature conditions can be used to determine the material constants of the constitutive equation. The hyperbolic sine-type equation Eq 1, which was proposed by Sellars and McTegart (Ref 6), has been widely adopted to

characterize the relationship between deformation parameters and specimen response over a wide range of stresses:

$$\dot{\varepsilon} = A[\sinh(\alpha\sigma)]^n \exp\left(\frac{-Q}{RT}\right) \qquad (\text{Eq 1})$$

where A (s^{-1}), α (MPa^{-1}) and n (stress exponent) are material constants, $\dot{\varepsilon}$ is the strain rate (s^{-1}), R is the universal gas constant (8.314 J/mol/K), σ is the flow stress (MPa), and Q is the activation energy for deformation (J/mol).

The value of the constant α is derived by the division of β and n_1 (Ref 13), which are material constants in the two limited conventional constitutive equations, i.e. the exponential law which is suitable at higher stresses Eq 2 and the power law which is applicable to lower stresses (Eq 3) (Ref 34):

$$\dot{\varepsilon} = A_2 \exp(\beta\sigma) \qquad (\text{Eq 2})$$

$$\dot{\varepsilon} = A_1 \sigma^{n_1} \qquad (\text{Eq 3})$$

where A_1, n_1, β, and A_2 are material constants. Taking natural logarithm of both sides of Eqs 2 and 3 at a constant temperature respectively yields:

$$\sigma = \frac{1}{\beta} \ln \dot{\varepsilon} - \frac{1}{\beta} \ln A_2 \qquad (\text{Eq 4})$$

$$\ln \sigma = \frac{1}{n_1} \ln \dot{\varepsilon} - \frac{1}{n_1} \ln A_1 \qquad (\text{Eq 5})$$

Substituting the values of the flow stress and corresponding strain rate under the strain of 0.1 into the Eqs 4 and 5 gives the relationship between the flow stress and strain rate, as shown in Fig. 4. The value of β and n_1 are obtained as 0.19298 and 6.41922 from the slope of the lines in the $\sigma - \ln \dot{\varepsilon}$ and $\ln \sigma - \ln \dot{\varepsilon}$ plots, respectively. Hence, the value of the constant α at the strain of 0.1 is calculated to be 0.03006 MPa^{-1}.

Taking natural logarithm from both sides of Eq 1 and rearranging them the following equation is derived:

$$\ln[\sinh(\alpha\sigma)] = \frac{\ln \dot{\varepsilon}}{n} + \frac{Q}{nRT} - \frac{\ln A}{n} \qquad (\text{Eq 6})$$

At the given true strain ($\varepsilon = 0.1$), substituting the value of flow stress and the corresponding strain rate into Eq 6, the

value of n can be derived from the average slopes of the lines in $\ln[\sinh(\alpha\sigma)] - \ln \dot{\varepsilon}$ plots (Fig. 5) at all temperature levels. Assuming $\alpha = 0.03006$, the value of n is calculated to be 6.42 at the true strain of 0.1.

At a constant strain rate, the partial differentiation of Eq 1 with respect to $1/T$, leads to the following equation:

$$\frac{Q}{nRT} = \left[\frac{\partial \ln[\sinh(\alpha\sigma)]}{\partial\left(\frac{1}{T}\right)} \right]_{\dot{\varepsilon}} \qquad (\text{Eq 7})$$

According to Eq 7, the activation energy (Q) is determined from the slope of $\ln[\sinh(\alpha\sigma)]$ versus $1/T$ (Fig. 6), through averaging the slope values at different strain rates. Considering $n = 6.42$ and $R = 8.314$ J/mol/K, the Q value found at the true strain of 0.1 is obtained as 556.48 kJ/mol. This value for the activation energy deviates largely from the activation energy for self-diffusion in austenite [285 kJ/mol (Ref 35)], and is in agreement with other results on microalloyed steels
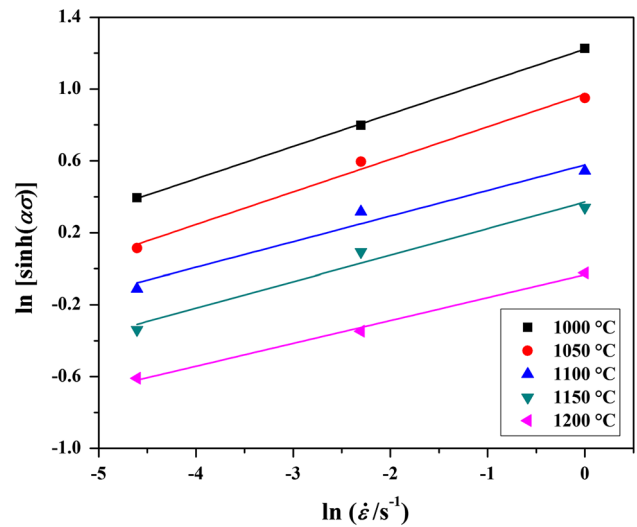

Fig. 5 The relationships between $\ln[\sinh(\alpha\sigma)]$ and $\ln \dot{\varepsilon}$ at different temperatures, assuming $\alpha = 0.03006$ MPa^{-1}
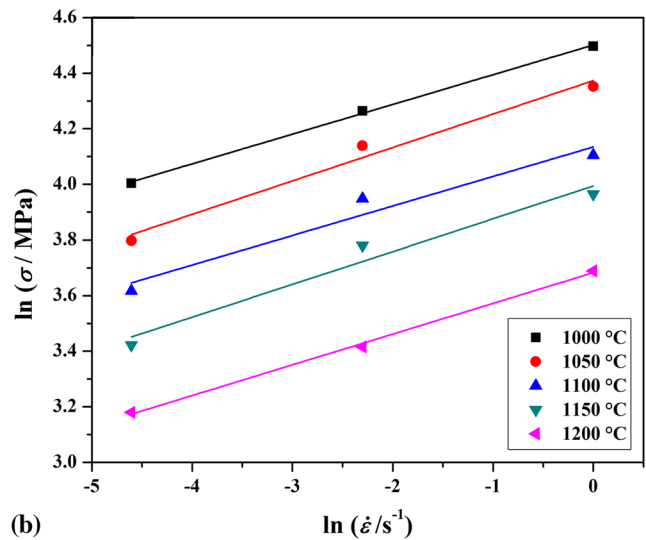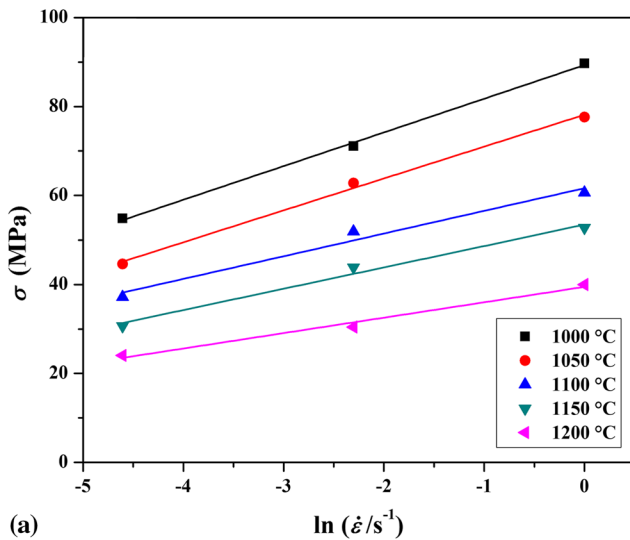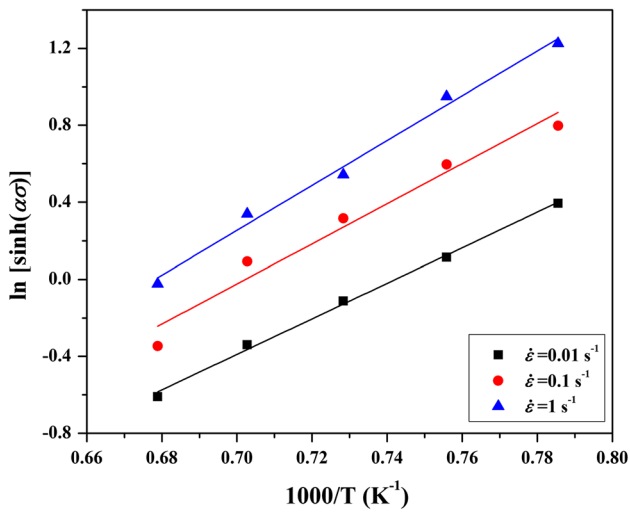

Fig. 4 The relationship between flow stresses and strain rates at the true strain of 0.1 according to the (a) exponential law and (b) power law

Fig. 6 The relationships between $\ln[\sinh(\alpha\sigma)]$ and $1/T$ at different strain rates, assuming $\alpha = 0.03006$ MPa^{-1}

(Ref 20, 30, 32, 36). Furthermore, comparing this value with the deformation activation energy of other microalloyed steels [305 kJ/mol (Ref 36), 393 kJ/mol (Ref 20), 375 kJ/mol (Ref 32) and 386 kJ/mol (Ref 30)] and C-Mn steels [338 kJ/mol (Ref 37) and 271.93 kJ/mol (Ref 38)] indicates that the activation energy significantly increases with the addition of niobium and vanadium. The existence of these elements and their carbo-nitride precipitation significantly affects the motion of dislocations and subgrain boundaries, leading to strong retardation in the process of DRV and the initiation of DRX (Ref 39). The calculated activation energy for the investigated material is comparable to the activation energy of 316 stainless steel (Ref 34).

Furthermore, the value of $\ln A$ can be derived by substituting the obtained values of the stress exponent, stress multiplier and activation energy for all tested temperatures at the true strain of 0.1 into Eq 6. The value of $\ln A$ at the true strain of 0.1 is calculated to be 45.493.
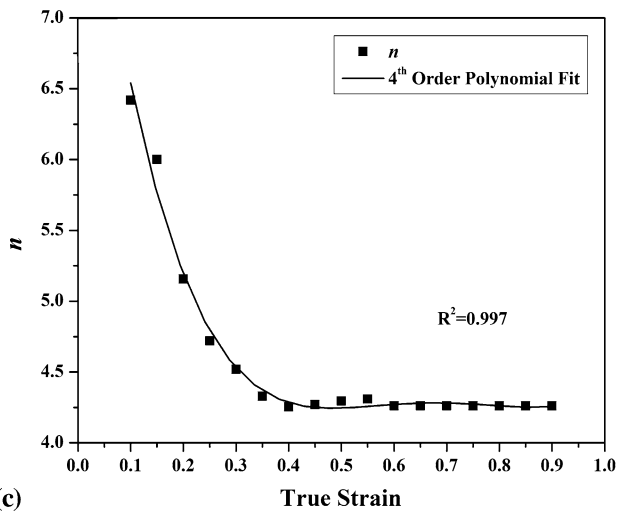
This procedure has been executed to find the material parameters at various strains in the range of 0.1-0.9 with an interval of 0.05. Figure 7 shows the variations of the material
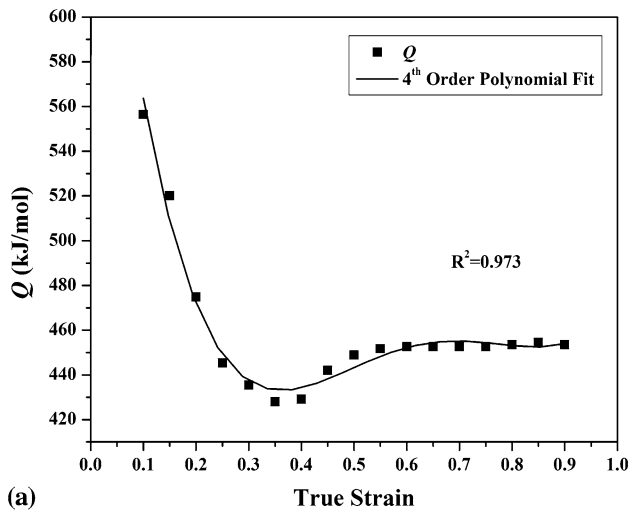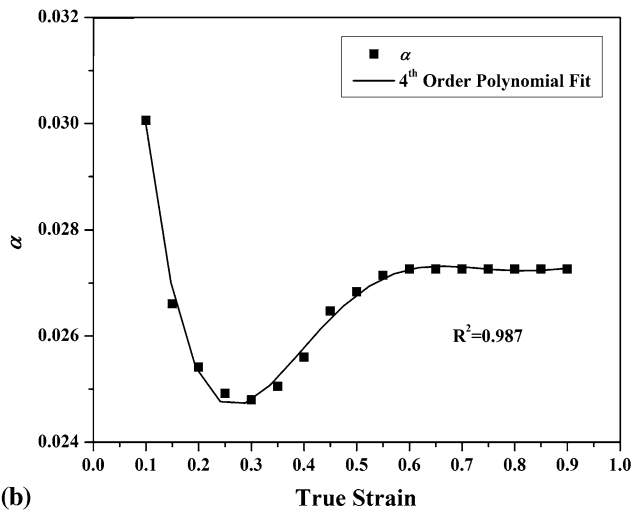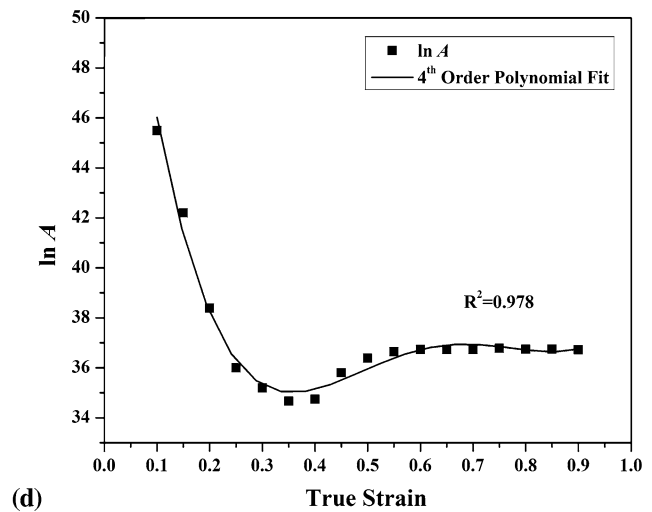

Fig. 7 The variations of material constants (a) Q, (b) α, (c) n and (d) $\ln A$ as a function of true strain using a fourth order polynomial fit for the investigated microalloyed steel

constants (α, n, Q and ln A) with true strain. The material parameters display significant dependence on the amount of strain. The value of each material parameter drops gradually to a relatively steady amount as the deformation proceeds (i.e., as true strain increases). Hence, in order to predict the flow stress more precisely and accurately, the compensation of strain should be taken into account when evaluating the constitutive equation (Ref 5). To this end, the material parameters (α, n, Q and ln A) are represented as polynomial functions of strain (Ref 40). The calculated values for each material parameter in Fig. 7 suggest that the fourth order polynomial functions (given by Eqs 8-11) represent an appropriate correlation between each material parameter and true strain. The coefficients of the fourth order polynomial functions are shown in Table 2.

$$\alpha = \alpha_0 + \alpha_1\varepsilon + \alpha_2\varepsilon^2 + \alpha_3\varepsilon^3 + \alpha_4\varepsilon^4 \qquad (\text{Eq 8})$$

$$Q = Q_0 + Q_1\varepsilon + Q_2\varepsilon^2 + Q_3\varepsilon^3 + Q_4\varepsilon^4 \qquad (\text{Eq 9})$$

$$n = n_0 + n_1\varepsilon + n_2\varepsilon^2 + n_3\varepsilon^3 + n_4\varepsilon^4 \qquad (\text{Eq 10})$$

$$\ln A = A_0 + A_1\varepsilon + A_2\varepsilon^2 + A_3\varepsilon^3 + A_4\varepsilon^4 \qquad (\text{Eq 11})$$

Once the material parameters with the compensation of strain are evaluated, the flow stress in the temperature range of 1000-1200 °C and under strain rates of 0.01, 0.1 and 1 s^{-1} can be calculated at a particular strain, using the following equation (Ref 13):

$$\sigma = \frac{1}{\alpha(\varepsilon)} \ln \left\{ \left(\frac{Z_{[Q(\varepsilon)]}}{A(\varepsilon)} \right)^{\frac{1}{n(\varepsilon)}} + \sqrt{\left(\frac{Z_{[Q(\varepsilon)]}}{A(\varepsilon)} \right)^{\frac{2}{n(\varepsilon)}} + 1} \right\} \qquad (\text{Eq 12})$$

where $Z = \dot{\varepsilon} \exp\left(\frac{Q}{RT}\right)$ is the Zener-Hollomon parameter and all material parameters calculated from Eqs 8-11.

3.3 Verification of the Developed Constitutive Model

To provide a better impression of the accuracy of the developed constitutive model with the compensation of strain for high temperature flow behavior of the investigated microalloyed steel, a comparison of the predicted flow stresses with the experimental ones in a wide range of strain, temperature and strain rate is carried out. Figure 8 depicts these comparisons. It can be seen that the developed constitutive model can efficiently predict the flow stress of the investigated material over the entire range of deformation conditions.

To provide better impression of the precision of the developed constitutive model, the predicted values of flow stress are plotted against the experimental ones in Fig. 9. It can be clearly observed that most of the data points lie fairly close to the best regression line and the square correlation coefficient

(R^2) for the developed constitutive model is 0.988, which indicates that a good correlation between the predicted and experimental data has been achieved.

To further assess the reliability of the developed constitutive model, the average absolute relative error (Δ) between the calculated flow stress and the experimental flow stress is calculated. This statistical parameter is given by:

$$\Delta(\%) = \frac{1}{N} \sum_{i=1}^{N} \left| \frac{\sigma_{\exp}^i - \sigma_p^i}{\sigma_{\exp}^i} \right| \times 100 \qquad (\text{Eq 13})$$

where $\sigma_{\exp}$ is the experimental flow stress, σ_p is the predicted flow stress and N is the total number of data points. The calculation result shows that the absolute average error in prediction for the entire range of deformation parameters is 6.08%, which also indicates that the developed constitutive model can effectively predict the high temperature flow behavior of the investigated microalloyed steel.

3.4 Analysis of DRX Behavior

3.4.1 Determination of Critical Characteristics of Dynamic Recrystallization. Using the true stress-true strain data, the values of the strain hardening rate ($\theta = \frac{d\sigma}{d\varepsilon}$) for different deformation conditions are calculated and plotted against the true stress in Fig. 10. It can be seen that θ varies with σ due to the effect of both DRV and DRX. According to the approach of Poliak and Jonas (Ref 21, 41, 42), the point on the θ-σ curves at which the work hardening rate equals zero ($\theta = 0$) represents the peak stress (σ_p) and the inflection point of the curves indicates the critical stress for the initiation of DRX (σ_c). The value of peak (ε_p) and critical strains (ε_c) can be defined by mapping the peak and critical stresses back onto the stress-strain curves (Ref 14).

Najafizadeh and Jonas (Ref 24) have reported that the θ-σ curve up to the peak stress can be well described by a third order polynomial equation given by:

$$\theta = a\sigma^3 + b\sigma^2 + c\sigma + d \qquad (\text{Eq 14})$$

where a, b, c and d are constant parameters for each deformation condition.

If one differentiates Eq 14 twice with respect to σ, the following equation is obtained:

$$\frac{d^2\theta}{d\sigma^2} = 6a\sigma + 2b \qquad (\text{Eq 15})$$

Therefore, the critical stress for initiation of DRX results by setting the Eq 15 equal to zero:

$$\sigma_c = \frac{-b}{3a} \qquad (\text{Eq 16})$$

The results of peak and critical stresses and strains for the temperatures of 1000, 1100 and 1200 °C under different strain rates of 0.01, 0.1 and 1 s^{-1} are summarized in Table 3.

According to Table 3, at a constant temperature, the critical and peak stresses and strains increase with an increase of the strain rate. However, at a constant strain rate, these parameters increase as the deformation temperature decreases. The average ratio of $\varepsilon_c/\varepsilon_p$ and σ_c/σ_p are 0.37 and 0.81, respectively. Similar results have been reported by Xu et al. (Ref 20). Comparing these values with the values reported for stainless steel [$\varepsilon_c/\varepsilon_p = 0.47$ and $\sigma_c/\sigma_p = 0.90$ (Ref 19)] indicates that DRX

Table 2 The coefficients of the fourth order polynomial function for α, Q, n and ln A

α, MPa^{-1}	Q, KJ/mol	n	ln$A$
$\alpha_0 = 0.040$	$Q_0 = 745.42$	$n_0 = 8.909$	$A_0 = 61.64$
$\alpha_1 = -0.145$	$Q_1 = -2392.76$	$n_1 = -30.057$	$A_1 = -206.17$
$\alpha_2 = 0.461$	$Q_2 = 6435.81$	$n_2 = 70.630$	$A_2 = 559.71$
$\alpha_3 = -0.574$	$Q_3 = -7118.87$	$n_3 = -71.591$	$A_3 = -623.53$
$\alpha_4 = 0.247$	$Q_4 = 2802.51$	$n_4 = 26.485$	$A_4 = 246.68$
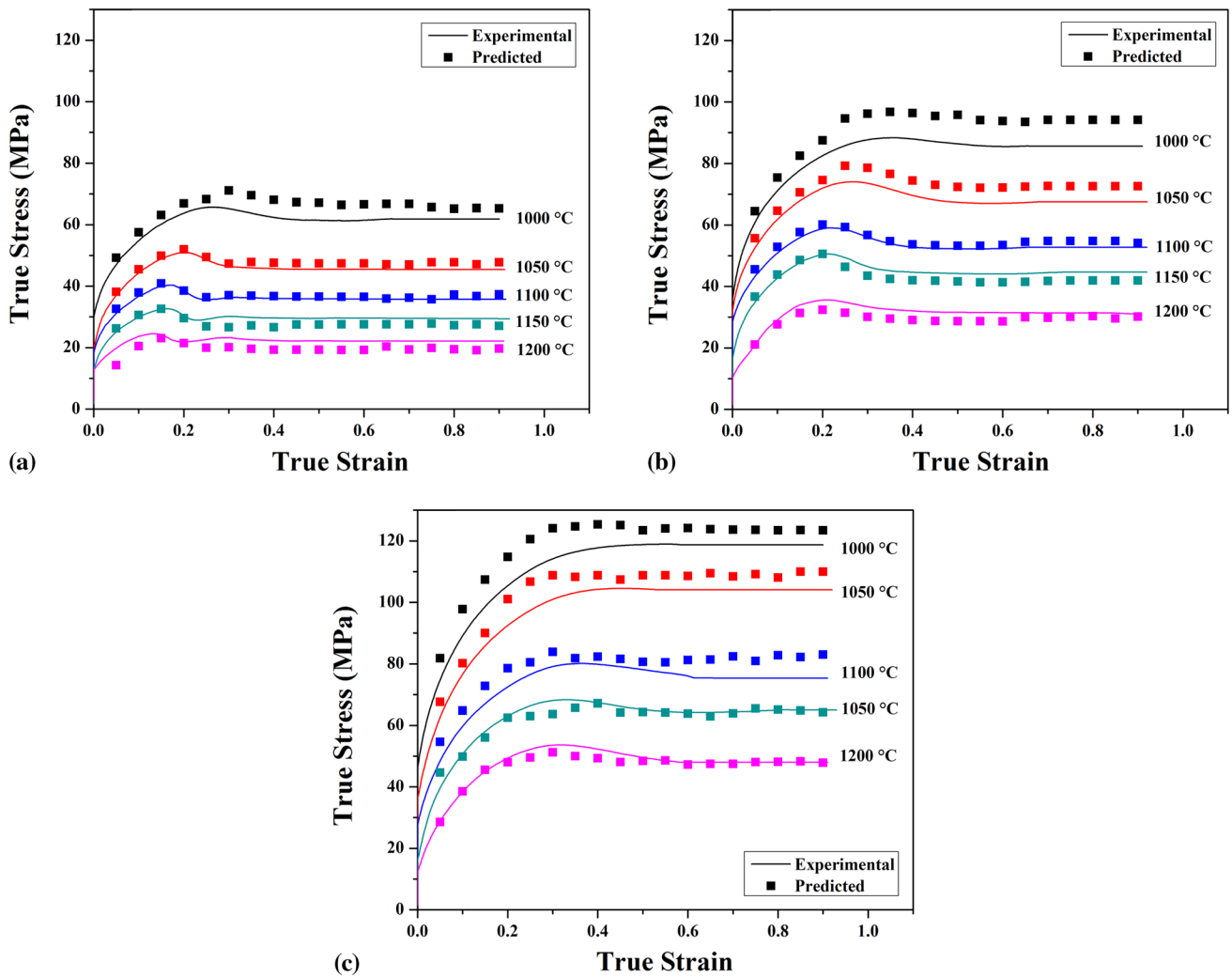
Fig. 8 Comparison between the experimental and predicted flow stresses at different temperatures under strain rates of (a) 0.01, (b) 0.1, (c) 1 s^{-1}
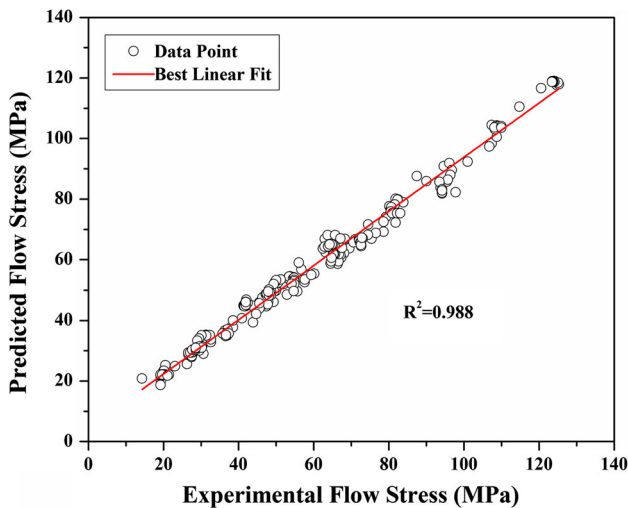
Fig. 9 Correlation between experimental and predicted flow stresses at the chosen deformation conditions

is likely to occur in the present microalloyed steel. This may be attributed to the effect of microalloying elements on the motion of dislocation and subgrain boundaries.

Figure 11 illustrates the dependence of critical and peak stresses and their corresponding strains on the Zener-Hollomon parameter and, also, the linear regression results. It can be seen that the critical characteristics of DRX increase with increasing Z parameter. The relationship between these parameters and deformation conditions (Z) is expressed by a power law equation (AZ^m, where A is a constant depending on the chemical composition and the initial grain size of material and m is a power law exponent) (Ref 32, 43). According to the linear regression results shown in Fig. 11, the following equations hold for the investigated steel:

$$\sigma_p = 0.1826Z^{0.1507} \qquad (Eq\ 17)$$

$$\varepsilon_p = 0.0017Z^{0.1324} \qquad (Eq\ 18)$$

$$\sigma_c = 0.1362Z^{0.1528} \qquad (Eq\ 19)$$
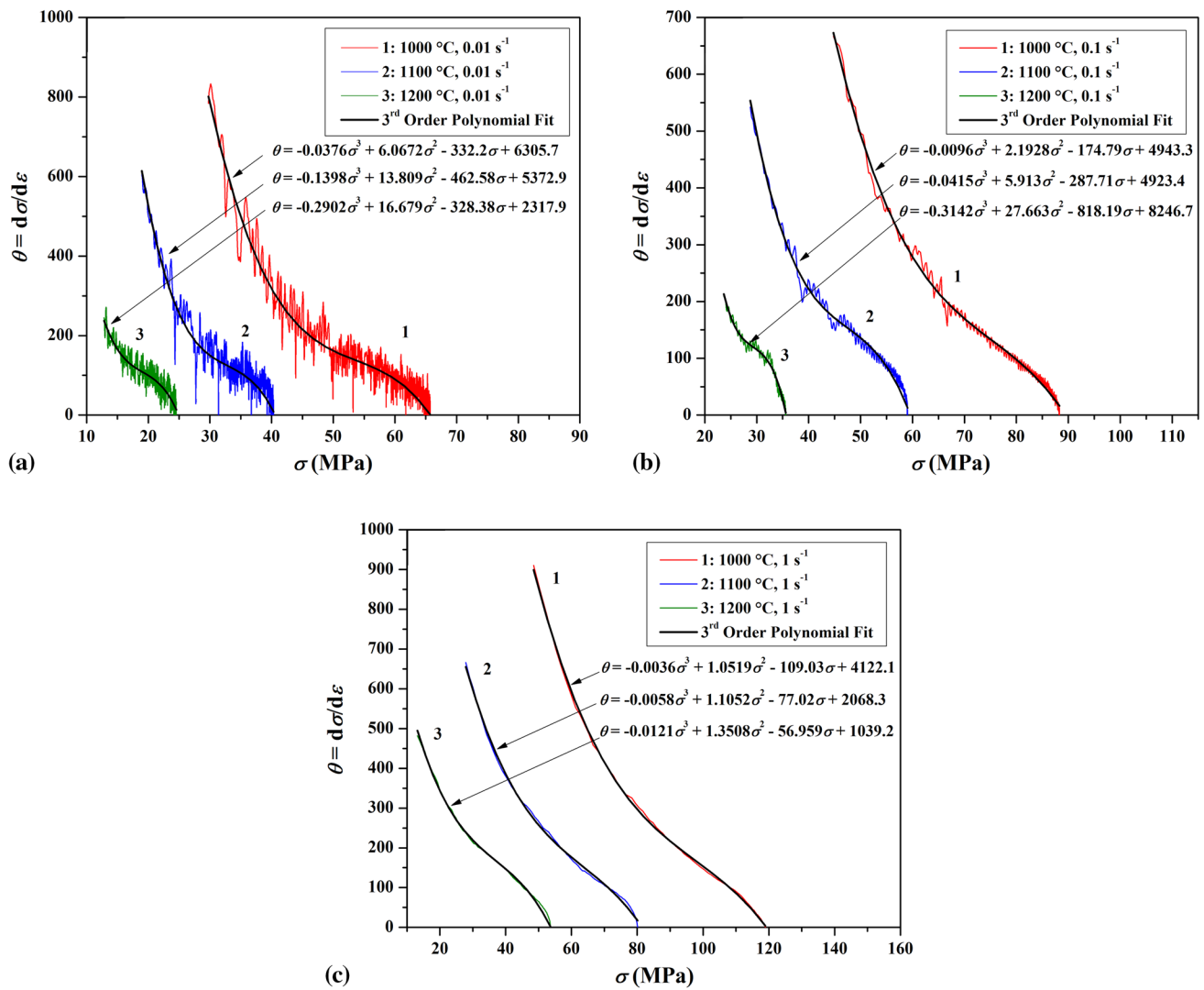
Fig. 10 θ-σ curves of the microalloyed steel under hot deformation conditions at different temperatures and strain rates of (a) 0.01 s⁻¹, (b) 0.1 s⁻¹ and (c) 1 s⁻¹

Table 3 Critical and peak stresses and strains at different deformation conditions

Temperature	1000			1100			1200		
Strain rate	0.01	0.1	1	0.01	0.1	1	0.01	0.1	1
σ_p	65.72	88.05	118.95	40.35	59.05	80.11	24.51	35.60	53.60
ε_p	0.26	0.39	0.56	0.17	0.22	0.36	0.13	0.21	0.31
σ_c	53.79	75.12	97.69	35.93	47.45	63.37	19.15	29.36	37.48
ε_c	0.09	0.13	0.14	0.09	0.08	0.12	0.04	0.10	0.09
$\varepsilon_c/\varepsilon_p$	0.35	0.33	0.26	0.53	0.35	0.34	0.34	0.49	0.31
σ_c/σ_p	0.82	0.85	0.82	0.89	0.80	0.79	0.78	0.82	0.70

$$\varepsilon_c = 3.041 Z^{0.0903} \qquad \text{(Eq 20)}$$

The dependence of these critical characteristics of DRX on temperature and strain rate lends support to the conclusion that the deformation is controlled by a thermally activated process (Ref 32).

3.4.2 The Kinetics of DRX. It has been reported that the volume fraction of dynamically recrystallized grains (X) can be derived from the flow curves (Ref 19, 25, 44). In this study, due to the relatively low stacking fault energy of austenite, the effect of DRV on flow softening was not considered (Ref 19, 25). Therefore, the flow softening was directly related to the
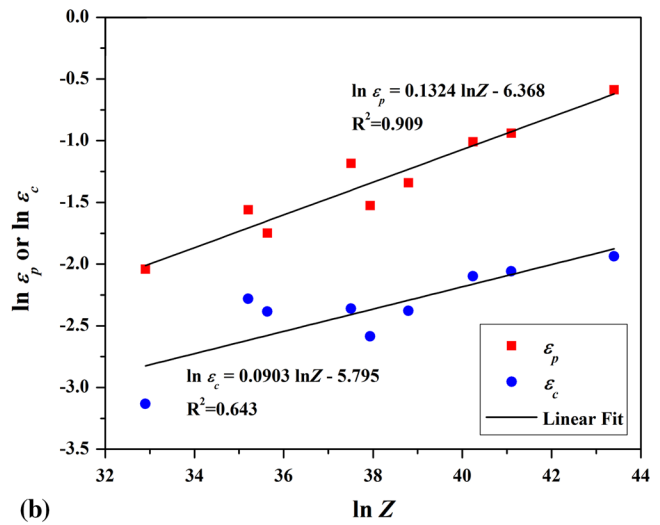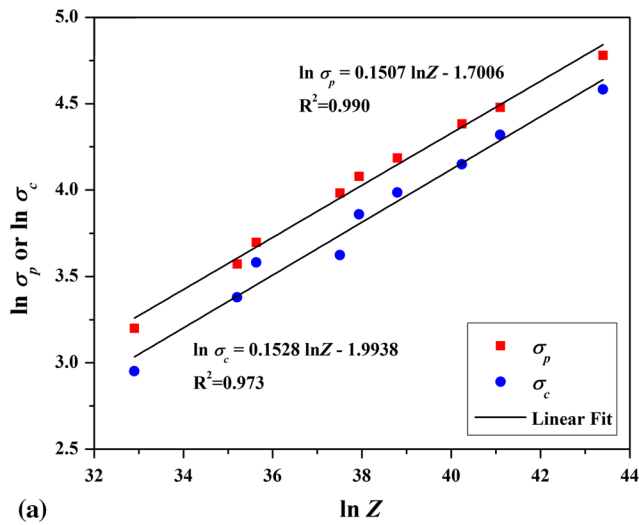
Fig. 11 The relation between (a) σ_c, σ_p and (b) ε_c, ε_p with Z parameter, assuming $Q = 459.33$ kJ mol^{-1} (picking other values for Q entails a modification of the parameters A and n in Eqs 17-20)
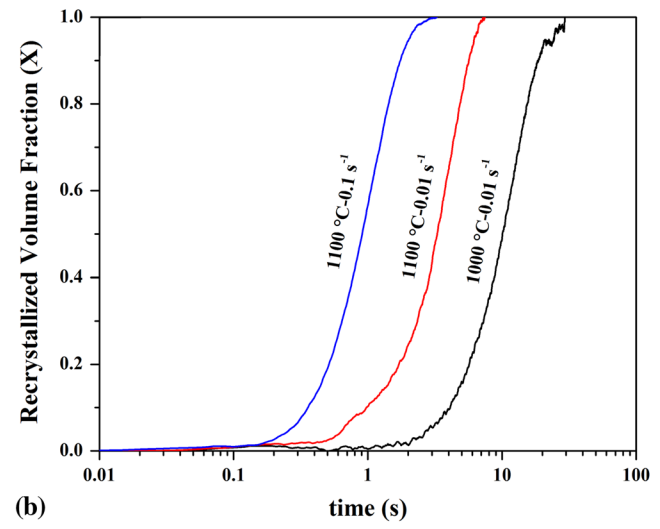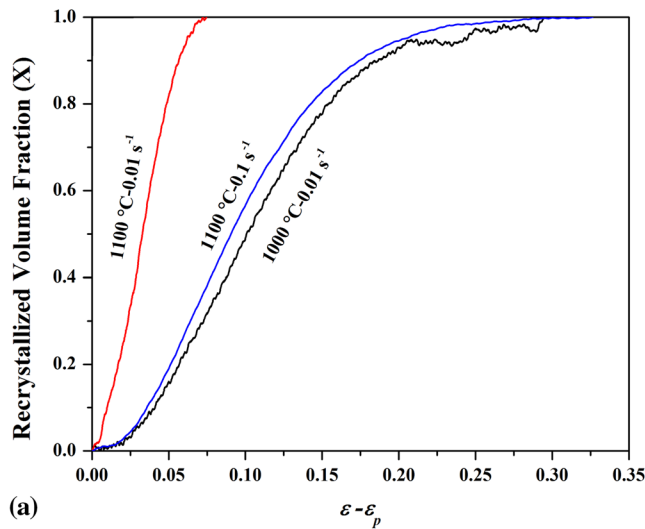
Fig. 12 Effect of deformation temperature and strain rate on the kinetics of DRX, (a) recrystallized volume fraction (X) versus strain, (b) X versus time

volume fraction of DRX which is calculated from Eq 21 (Ref 19). In this equation, the σ_p-σ term indicates the flow softening from the peak stress to σ and the σ_p-σ_s term represents the maximum achievable softening (Ref 19). It should be mentioned that in this model the initiation of DRX was considered to occur at the peak stress (Ref 19). Moreover, the DRX time (t) from peak strain (ε_p) to strain of ε may be determined by Eq 22 (Ref 19).

$$X = \frac{\sigma_p - \sigma}{\sigma_p - \sigma_s} \qquad (Eq\ 21)$$

$$t = \frac{\varepsilon - \varepsilon_p}{\dot{\varepsilon}} \qquad (Eq\ 22)$$

Figure 12 shows the kinetics of DRX at different deformation conditions, using Eqs 21 and 22. These figures show that the DRX volume fraction (X) increases with strain and

recrystallization time until a fully recrystallized microstructure is achieved by continuous nucleation and grain boundary migration (Ref 45). According to Fig. 12a, by increasing strain rate at the constant temperature of 1100 °C or decreasing deformation temperature under constant strain rate of 0.01 s^{-1}, the recrystallization curve is shifted to the higher strains. Moreover, Fig. 12b illustrates this shift in terms of recrystallization times, which clearly demonstrates that the kinetics of DRX increases with increasing deformation temperature or strain rate.

4. Conclusions

In this study, the hot deformation behavior of a medium carbon microalloyed steel has been investigated using hot

compression test in the temperature range of 1000-1200 °C and under different strain rates of 0.01, 0.1 and 1 s^{-1}. The key results of this investigation are as follows:

1. The flow stress is strongly dependent on deformation temperature and strain rate and is seen to increase with decreasing temperature and increasing strain rate. Moreover, the investigated microalloyed steel shows cyclic flow behavior at the deformation temperatures of 1100, 1150 and 1200 °C under the strain rate of 0.01 s^{-1}, associated with grain coarsening during DRX. Furthermore, DRX is found to be the main flow softening mechanism in almost all deformation conditions.
2. The material parameters in the hyperbolic sine constitutive equation (Q, n, A, and α) are found to be strain dependent and the functional relations between material constants and strain are identified by a fourth order polynomial fit.
3. The constitutive model incorporating the effect of strain achieves a good match to the experimentally recorded flow stress of the investigated alloy. The accuracy of the proposed model is evaluated by applying the absolute average error method with an error of 6.08%, indicating a good agreement between predicted and experimental flow stresses.
4. The critical characteristics of DRX (σ_p, ε_p, σ_c, ε_c) at different deformation conditions are extracted from the stress-strain curves, using the strain hardening parameter. Also, the relationships between these parameters and the Zener-Hollomon (Z) are expressed as power law equations.
5. By increasing the strain rate at a constant temperature or decreasing deformation temperature under a constant strain rate, the recrystallization curve shifts to higher strains. However, the kinetics of DRX increases with increasing deformation temperature or strain rate.

References

1. H.H. Bok, M.G. Lee, H.D. Kim, and M.B. Moon, Thermo-Mechanical Finite Element Analysis Incorporating the Temperature Dependent Stress-Strain Response of Low Alloy Steel for Practical Application to the Hot Stamped Part, *Met. Mater. Int.*, 2010, **16**, p 185–195
2. M.A. Bonte, L. Fourment, T.T. Do, A.H. Boogaard, and J. Huétink, Optimization of Forging Processes Using Finite Element Simulations, *Struct. Multidiscip. Optim.*, 2010, **42**, p 797–810
3. A.R. Shahani, S. Setayeshi, S.A. Nodamaie, M.A. Asadi, and S. Rezaie, Prediction of Influence Parameters on the Hot Rolling Process Using Finite Element Method and Neural Network, *J. Mater. Process Technol.*, 2009, **209**, p 1920–1935
4. Y.C. Lin, M.S. Chen, and J. Zhong, Constitutive Modeling for Elevated Temperature Flow Behavior of 42CrMo Steel, *Comput. Mater. Sci.*, 2008, **42**, p 470–477
5. Y.C. Lin and X.M. Chen, A Critical Review of Experimental Results and Constitutive Descriptions for Metals and Alloys in Hot Working, *Mater. Des.*, 2011, **32**, p 1733–1759
6. C.M. Sellars and W.J. McTegart, On the Mechanism of Hot Deformation, *Acta Metal.*, 1966, **14**, p 1136–1138
7. L.X. Li, Y. Lou, L.B. Yang, D.S. Peng, and K.P. Rao, Flow Stress Behavior and Deformation Characteristics of Ti-3Al-5V-5Mo Compressed at Elevated Temperatures, *Mater. Des.*, 2002, **23**, p 451–457
8. A. Momeni, H. Arabi, A. Rezaei, H. Badri, and S.M. Abbasi, Hot Deformation Behavior of Austenite in HSLA-100 Microalloyed Steel, *Mater. Sci. Eng. A*, 2011, **528**, p 2158–2163
9. K.P. Rao, Y.K.D.V. Prasad, and E.B. Hawbolt, Hot Deformation Studies on a Low-Carbon Steel: Part 1—Flow Curves and the Constitutive Relationship, *J. Mater. Process Technol.*, 1996, **56**, p 897–907
10. J. Cai, F. Li, T. Liu, B. Chen, and M. He, Constitutive Equations for Elevated Temperature Flow Stress of Ti-6Al-4V Alloy Considering the Effect of Strain, *Mater. Des.*, 2011, **32**, p 1144–1151
11. P. Changizian, A. Zarei-Hanzaki, and A.A. Roostaei, The High Temperature Flow Behavior Modeling of AZ81 Magnesium Alloy Considering Strain Effects, *Mater. Des.*, 2012, **39**, p 384–389
12. Y. Han, G. Qiao, Y. Sun, and D. Zou, Modeling the Constitutive Relationship of Cr20Ni25Mo4Cu Superaustenitic Stainless Steel During Elevated Temperature, *Mater. Sci. Eng. A*, 2012, **539**, p 61–67
13. S. Mandal, V. Rakesh, P.V. Sivaprasad, S. Venugopal, and K.V. Kasiviswanathan, Constitutive Equations to Predict High Temperature Flow Stress in a Ti-Modified Austenitic Stainless Steel, *Mater. Sci. Eng. A*, 2009, **500**, p 114–121
14. G.R. Stewart, A.M. Elwazri, S. Yue, and J.J. Jonas, Modelling of Dynamic Recrystallisation Kinetics in Austenitic Stainless and Hypereutectoid Steels, *Mater. Sci. Technol.*, 2006, **22**, p 519–524
15. J.H. Bianchi and L.P. Karjalainen, Modelling of Dynamic and Metadynamic Recrystallisation During Bar Rolling of a Medium Carbon Spring Steel, *J. Mater. Process. Technol.*, 2005, **160**, p 267–277
16. S.I. Kim, Y. Lee, and S.M. Byon, Study on Constitutive Relation of AISI, 4140 Steel Subject to Large Strain at Elevated Temperatures, *J. Mater. Process. Technol.*, 2003, **140**, p 84–89
17. A. Momeni, S.M. Abbasi, and H. Badri, Hot Deformation Behavior and Constitutive Modeling of VCN200 Low Alloy Steel, *Appl. Math. Model.*, 2012, **36**, p 5624–5632
18. A. Momeni, K. Dehghani, H. Keshmiri, and G.R. Ebrahimi, Hot Deformation Behavior and Microstructural Evolution of a Superaustenitic Stainless Steel, *Mater. Sci. Eng. A*, 2010, **527**, p 1605–1611
19. H. Mirzadeh and A. Najafizadeh, Prediction of the Critical Conditions for Initiation of Dynamic Recrystallization, *Mater. Des.*, 2010, **31**, p 1174–1179
20. Y. Xu, D. Tang, Y. Song, and X. Pan, Dynamic Recrystallization Kinetics Model of X70 Pipeline Steel, *Mater. Des.*, 2012, **39**, p 168–174
21. E.I. Poliak and J.J. Jonas, A One-Parameter Approach to Determining the Critical Conditions for the Initiation of Dynamic Recrystallization, *Acta Mater.*, 1996, **44**, p 127–136
22. X.G. Fan, H. Yang, Z.C. Sun, and D.W. Zhang, Quantitative Analysis of Dynamic Recrystallization Behavior Using a Grain Boundary Evolution Based Kinetic Model, *Mater. Sci. Eng. A*, 2010, **527**, p 5368–5377
23. A. Momeni, K. Dehghani, and G.R. Ebrahimi, Modeling the Initiation of Dynamic Recrystallization Using a Dynamic Recovery Model, *J. Alloy Compd.*, 2011, **509**, p 9387–9393
24. A. Najafizadeh and J.J. Jonas, Predicting the Critical Stress for Initiation of Dynamic Recrystallization, *ISIJ Int.*, 2006, **46**, p 1679–1684
25. J.J. Jonas, X. Quelennec, L. Jiang, and É. Martin, The Avrami Kinetics of Dynamic Recrystallization, *Acta Mater.*, 2009, **57**, p 2748–2756
26. H.J. McQueen, Development of Dynamic Recrystallization Theory, *Mater. Sci. Eng. A*, 2004, **387-389**, p 203–208
27. H. Mirzadeh and A. Najafizadeh, The Rate of Dynamic Recrystallization in 17-4 PH Stainless Steel, *Mater. Des.*, 2010, **31**, p 4577–4583
28. ASTM International E209, Standard Practice for Compression Tests of Metallic Materials at Elevated Temperatures with Conventional or Rapid Heating Rates and Strain Rates. Annual Book of ASTM Standards, Vol 03.01, 2010
29. I. Tamura, *Thermomechanical Processing of High-Strength Low-Alloy Steels*, Butterworths, London, 1988
30. A.M. Elwazri, P. Wanjara, and S. Yue, Dynamic Recrystallization of Austenite in Microalloyed High Carbon Steels, *Mater. Sci. Eng. A*, 2003, **339**, p 209–215
31. D. Nakhaie, P. Hosseini Benhangi, F. Fazeli, M. Mazinani, E. Zohourvahid Karimi, M.R. Ghandehari Ferdowsi, Controlled Forging of a Nb Containing Microalloyed Steel for Automotive Applications, Metal. Mater. Trans. A, 2012, **43**, 5209–5217
32. M. Shaban and B. Eghbali, Determination of Critical Conditions for Dynamic Recrystallization of a Microalloyed Steel, *Mater. Sci. Eng. A*, 2010, **527**, p 4320–4325
33. T. Sakai, M.G. Akben, and J.J. Jonas, Dynamic Recrystallization During the Transient Deformation of a Vanadium Microalloyed Steel, *Acta Metall.*, 1983, **31**, p 631–641

34. H.J. McQueen and N.D. Ryan, Constitutive Analysis in Hot Working, *Mater. Sci. Eng. A*, 2002, **322**, p 43–63

35. E. Evangelista, M. Masini, M. El Mehtedi, and S. Spigarelli, Hot Working and Multipass Deformation of a 41Cr4 Steel, *J. Alloy Compd.*, 2004, **378**, p 151–154

36. D. Rasouli, S.K. Asl, A. Akbarzadeh, and G.H. Daneshi, Optimization of Mechanical Properties of a Micro Alloyed Steel, *Mater. Des.*, 2009, **30**, p 2167–2172

37. S. Serajzadeh and A. Karimi Taheri, An Investigation on the Effect of Carbon and Silicon on Flow Behavior of Steel, *Mater. Des.*, 2002, **23**, p 271–276

38. S.F. Medina and C.A. Hernandez, General Expression of the Zener-Hollomon Parameter as a Function of the Chemical Composition of Low Alloy and Microalloyed Steels, *Acta Mater.*, 1996, **44**, p 137–148

39. S.-H. Cho, K.-B. Kang, and J.J. Jonas, The Dynamic, Static and Metadynamic Recrystallization of a Nb-Microalloyed Steel, *ISIJ Int.*, 2001, **41**, p 63–69

40. Y.C. Lin, M.S. Chen, and J. Zhong, Effect of Temperature and Strain Rate on the Compressive Deformation Behavior of 42CrMo Steel, *J. Mater. Process. Technol.*, 2008, **205**, p 308–315

41. E.I. Poliak and J.J. Jonas, Critical Strain for Dynamic Recrystallization in Variable Strain Rate Hot Deformation, *ISIJ Int.*, 2003, **43**, p 692–700

42. E.I. Poliak and J.J. Jonas, Initiation of Dynamic Recrystallization in Constant Strain Rate Hot Deformation, *ISIJ Int.*, 2003, **43**, p 684–691

43. A. Dehghan-Manshadi, M.R. Barnett, P.D. Hodgson, Hot Deformation and Recrystallization of Austenitic Stainless Steel: Part I. Dynamic Recrystallization, *Metal. Mater. Trans. A*, 2008, **39**, 1359-1370

44. H.L. Wei, G.Q. Liu, H.T. Zhao, and R.M. Kang, Hot Deformation Behavior of Two C-Mn-Si Based and C-Mn-Al Based Microalloyed High-Strength Steels: A Comparative Study, *Mater. Des.*, 2013, **50**, p 484–490

45. S.I. Kim, Y. Lee, D.L. Lee, and Y.C. Yoo, Modeling of AGS and Recrystallized Fraction of Microalloyed Medium Carbon Steel During Hot Deformation, *Mater. Sci. Eng. A*, 2003, **355**, p 384–393